Climate Change Intensifies Bridge Temperature: Evidence from 26 Years of Monitoring Data

Lu Zhang[1], Xiaoyou Wang[2], Zhi-Peng Chen[3], Jing Qiang[4], and Yong Xia[5*]

[1] Postdoctoral Fellow, Department of Civil and Environmental Engineering, The Hong Kong Polytechnic University, Hong Kong, China; Joint Research Centre for Marine Infrastructure, The Hong Kong Polytechnic University, Hong Kong, China. Email: lu1zhang@polyu.edu.hk

[2] Research Assistant professor, Department of Civil and Environmental Engineering, The Hong Kong Polytechnic University, Hong Kong, China; Joint Research Centre for Marine Infrastructure, The Hong Kong Polytechnic University, Hong Kong, China. Email: cexiaoyou.wang@polyu.edu.hk

[3] The Hong Kong–Zhuhai–Macao Bridge Authority, Zhuhai, China. Guangdong-Hong Kong Joint Laboratory for Marine Infrastructure. Email: jq@hzmbo.com

[4] Research Assistant Professor, Department of Civil and Environmental Engineering, The Hong Kong Polytechnic University, Hong Kong, China; Email: zhipeng.chen@polyu.edu.hk

[5] Professor, Department of Civil and Environmental Engineering, Otto Poon Research Institute for Climate-Resilient Infrastructure, The Hong Kong Polytechnic University, Hong Kong, China. Guangdong-Hong Kong Joint Laboratory for Marine Infrastructure. Email: ceyxia@polyu.edu.hk

* Corresponding author

Abstract: Global warming has been increasing during the past decades and has been observed from worldwide observation stations. However, its impacts on civil infrastructure have not been observed or recorded due to a shortage of long-term field measurement data. This study uses the 2132-m long Tsing Ma Bridge in Hong Kong as a testbed and investigates the effects of climate change on the long-span bridge using 26 years (1999–2024) of field monitoring data. It shows that the annual mean temperature of the bridge deck has increased by 0.28 ℃ per decade and the annual extreme temperatures have risen by 0.50 ℃ per decade. Moreover, the annual 90th percentile bridge temperature and the frequency of extreme heat events exhibit an increasing trend. The standardized regression analysis shows that the ambient air temperature dominates the bridge temperature change. Finally, heat-transfer analysis is conducted to calculate the temperature distribution of the bridge. The numerical and monitoring results confirm the bridge temperature rise during the past decades. This study, for the first time, provides the real evidence of climate warming's impacts on long-span bridges using 26 years of field monitoring data, the longest in the world. The results highlight the urgency of reducing greenhouse gas emissions and developing adaptation strategies to mitigate the effects of rising temperature on the safety and serviceability of infrastructure in a warming world.

Keywords: climate change; bridge temperature; temperature rising; long-term monitoring; climate risk

1 Introduction

Long-span bridges are a critical component of transportation infrastructure and play a vital role in regional economic development and public connectivity [1, 2]. They effectively overcome geographical barriers, shorten travel distances, and significantly improve transportation efficiency. For example, the Hong Kong–Zhuhai–Macao Bridge has shortened the travel time between Zhuhai and Hong Kong from approximately 4 hours to 30 minutes. It promotes economic integration in the Greater Bay Area and is expected to generate over HKD 40 billion in economic benefits in 20 years. By 2023, China had more than 1.07 million bridges, a 4.27% increase from the previous year. These data highlight the indispensable role of bridges in supporting national transportation networks and driving regional development.

Bridges are constantly subjected to environmental factors, including daily and seasonal fluctuations in air temperature and solar radiation [3–5]. These factors drive heat exchange between the bridge structure and its surroundings, resulting in non-uniform temperature distributions across the bridge [6–10]. Such temperature variations can lead to thermal displacements and strains, which also may alter the dynamic characteristics of bridges [11–20]. For instance, the temperature-induced mid-span deflection of the 1377 m-long main span of the Tsing Ma Bridge in Hong Kong could reach 2,313 mm annually [21]. Similarly, the Runyang Bridge experienced seasonal longitudinal displacements of around 500 mm [22]. Field studies have demonstrated that temperature effects can exert a greater influence on bridge behavior than operational loads. Consequently, as one of bridge main loads, understanding the effect of temperature on bridge performance is crucial for ensuring structural safety and

longevity.

Increasing climate change has a significant effect on critical infrastructure, including bridges [23–35]. Climate change affects bridge temperatures primarily through air temperature and solar radiation [36–39]. These factors contribute to different aspects of heat transfer. Air temperature mainly influences convective heat exchange, whereas solar radiation increases the absorbed energy of bridge exposed surfaces. Global mean surface air temperature increases markedly, reaching 1.43 ℃ above pre-industrial level [40–44]. A widespread increase in solar radiation has also been observed since the late 1980s [45, 46]. Some researchers have explored the effects of climate change on bridges [47–49]. These studies have relied on theoretical models because long-term observation data on bridges are lacking. In fact, long-term field observation practice only started in the 1990s thanks to the development of structural health monitoring (SHM) technology. However, most of SHM systems have only collected several years of data. The climate change-induced temperature variation of bridges during the period of several years may be less than 0.5 ℃, which may be masked by annual temperature variation and thus cannot be observed reliably.

Since its commissioning in 1997, the Tsing Ma Bridge in Hong Kong has been equipped with a cutting-edge SHM system, widely regarded as the world's first comprehensive long-term SHM system for bridges [50, 51]. Over decades of continuous operation, this system has generated a unique dataset that captures bridge performance across a timescale comparable to climate change. For the first time, this study examines the monitoring temperature data from the bridge spanning from 1999 to 2024. This 26-year dataset provides an unprecedented

89 opportunity to examine the effect of climate change on bridge temperatures. It also offers first-
90 hand data for future design and maintenance of bridges because almost all countries' bridge
91 design codes are based on historical data.

92 This study evaluates the effect of climate change on bridge temperatures using 26 years
93 of monitoring records from the SHM system of the Tsing Ma Bridge. First, we analyze decadal-
94 scale bridge temperature trends (including maximum, mean, and minimum), and investigate
95 seasonal variation patterns. Next, we focus on extreme temperatures, including shifts in the
96 90th percentile threshold for extreme heat events, changes in extreme event frequency, and
97 quantification of the effects of ambient air temperature and solar radiation on bridge
98 temperatures at different quantiles. Finally, we conduct heat-transfer analysis to calculate the
99 annual maximum temperature of the bridge deck and compare it with field monitoring data.
100 This firsthand monitoring data and numerical results confirm the effect of climate change on
101 civil infrastructure, underscoring the critical need to account for climate change in the design
102 and management of bridge infrastructure.
103

2 The SHM system of Tsing Ma Bridge

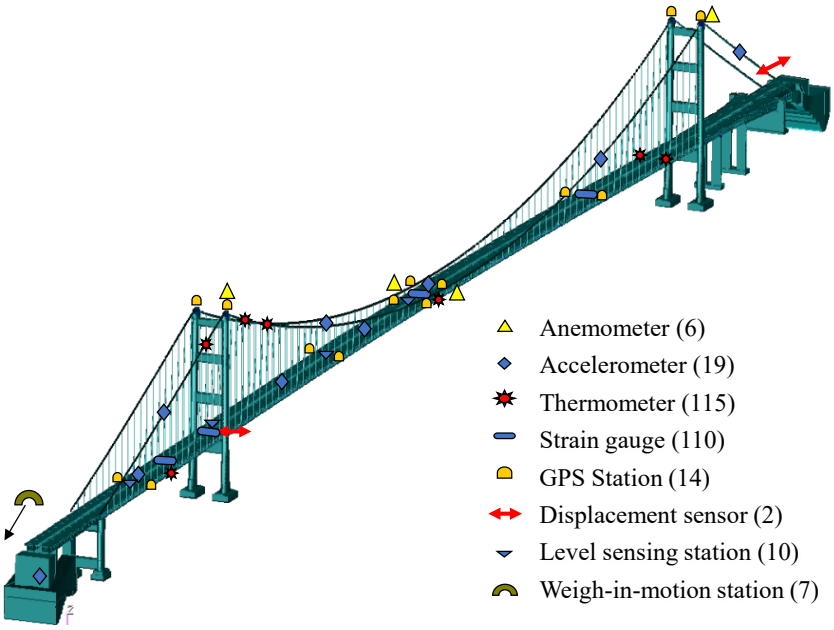

Figure 1 Layout of sensors on the Tsing Ma Bridge

Table 1 Sensors deployed on Tsing Ma Bridge

Monitoring Items	Sensor Types	No. of Sensors	Positions
Wind speed and direction	Anemometer	6	2: deck of main span; 2: top of towers; 2: deck of Ma Wan side span
Temperature	Thermometer	115	6: ambient; 23: main cables; 86: deck section
Highway traffic	Weigh-in-motion station	7	approach to Lantau Toll Plaza
Displacement	Displacement transducer	2	1: portal beam of Ma Wan tower; 1: deck at the Tsing Yi abutment
	GPS station	14	4: top of towers; 2: middle of main cables; 2: middle of the Ma Wan side span; 6: ¼, ½, and ¾ of the main span
	Level sensing station	10	1: abutment; 3: towers; 4: deck of the main span; 2: deck of the Ma Wan side span
Acceleration	Accelerometer	19	8: uniaxial, deck, and Tsing Yi tower; 9: biaxial, deck, and main cables; 2: triaxial, main cables, and the Ma Wan abutment
Strain	Strain gauge	110	29: Ma Wan side span; 49: main span; 32: cross frame at Ma Wan tower
Total		283	/

The Tsing Ma Bridge is a key component of the Lantau Link in Hong Kong, with a total length of 2,160 m connecting Tsing Yi Island and Ma Wan Island. This suspension bridge has a main span of 1,377 m supported by 206 m high towers. The Tsing Ma Bridge was officially opened on May 22, 1997, and it serves as a dual-use bridge, with the upper deck carrying highway traffic and the lower deck accommodating railways.

The bridge has been equipped with an SHM system since 1997, consisting of a total of 283 sensors [52]. These sensors include anemometers, thermometers, displacement transducer, level-sensing stations, GPS stations, accelerometers, strain gauges and weigh-in-motion stations. A total of 115 spatially distributed thermometers are positioned on the bridge's cable and deck to monitor temperatures. The layout of all sensors in the SHM system is shown in Figure 1, with all sensors summarized in Table 1.

The locations of thermometers measuring orthotropic deck (sensors A4 and B4) and U trough (sensors A1–A3 and B1–B3) temperatures are illustrated in Figure 2.

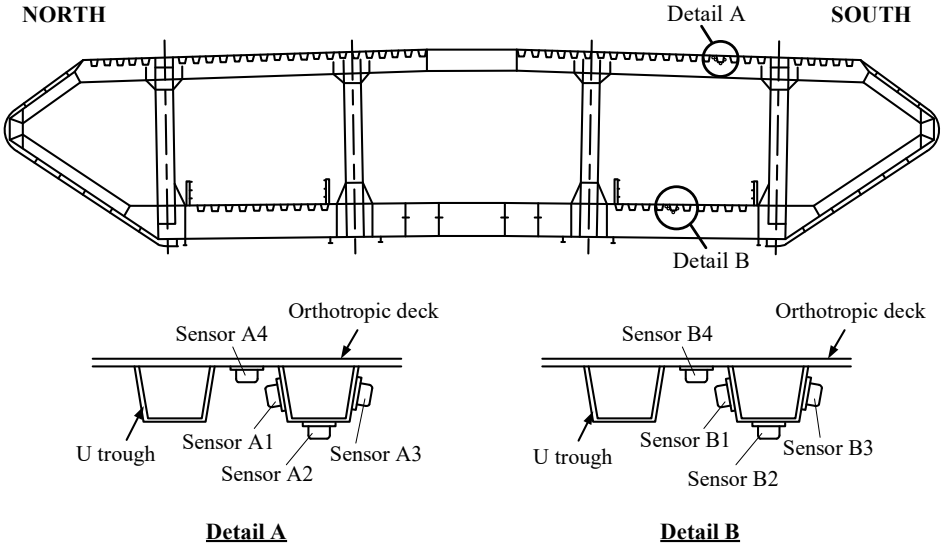

Figure 2 Locations of thermometers on bridge orthotropic deck and U trough

3 Changes in bridge effective temperatures

3.1 Effective temperature

Bridge cross-section consists of many components, each with different temperatures. Bridge design codes adopt the concept of effective bridge temperature to evaluate thermal effects. By computing a weighted average of temperatures measured at different locations across the bridge cross-section, the effective temperature can be calculated as follows [53]:

$$T_b = \frac{\sum_{i=1}^{n} T_i \times A_i}{\sum_{i=1}^{n} A_i}, \quad (1)$$

where T_b is the bridge effective temperature, T_i is the temperature of region i, A_i is the area around region i.

3.2 Bridge effective temperature trends

The effective temperatures derived from the SHM system of the Tsing Ma Bridge over the 26-year observational period (1999–2024) are studied, as shown in Figure 3. Figures 3(a), (b) and (c) are the annual maximum, mean and minimum temperature trends, respectively. In Figure 3(a), both bridge and air maximum temperatures show significant warming trends, at rates of 0.50 ℃ and 0.85 ℃ per decade respectively. The annual mean bridge effective temperature in Figure 3(b) shows a statistically significant increase of 0.28 ℃ per decade,

closely paralleling the concurrent ambient air temperature rise of 0.32 ℃ per decade. Notably, the annual maximum bridge temperature increase rate is 1.8 times the annual mean trend, highlighting disproportionate warming under extreme thermal conditions. In contrast, the annual minimum bridge temperature increase in Figure 3(c) is only 0.09 ℃ per decade, which is insignificant compared to the increases in the maximum and mean temperatures. In addition, the linear regression between the annual mean bridge effective temperature versus air temperature is studied and shown in Figure 3(d). It demonstrates a very strong linear relationship ($R^2 = 0.87$), indicating that bridge effective temperature is highly correlated with air temperature.

Subsequently, bridge temperature trends in different seasons are calculated. Figure 4 presents the seasonal warming rate and reveals divergent patterns. In Particular, autumn exhibits the most rapid temperature increase of 0.61 ℃ per decade, whereas spring shows a small decrease of –0.06 ℃ per decade. Summer and winter display moderate warming rates of 0.28 ℃ per decade and 0.32 ℃ per decade, respectively. These trends are also close to the rate of ambient air temperature changes across seasons, with corresponding rates of –0.01 ℃, 0.29 ℃, 0.59 ℃, and 0.38 ℃ per decade for spring, summer, autumn, and winter, respectively.

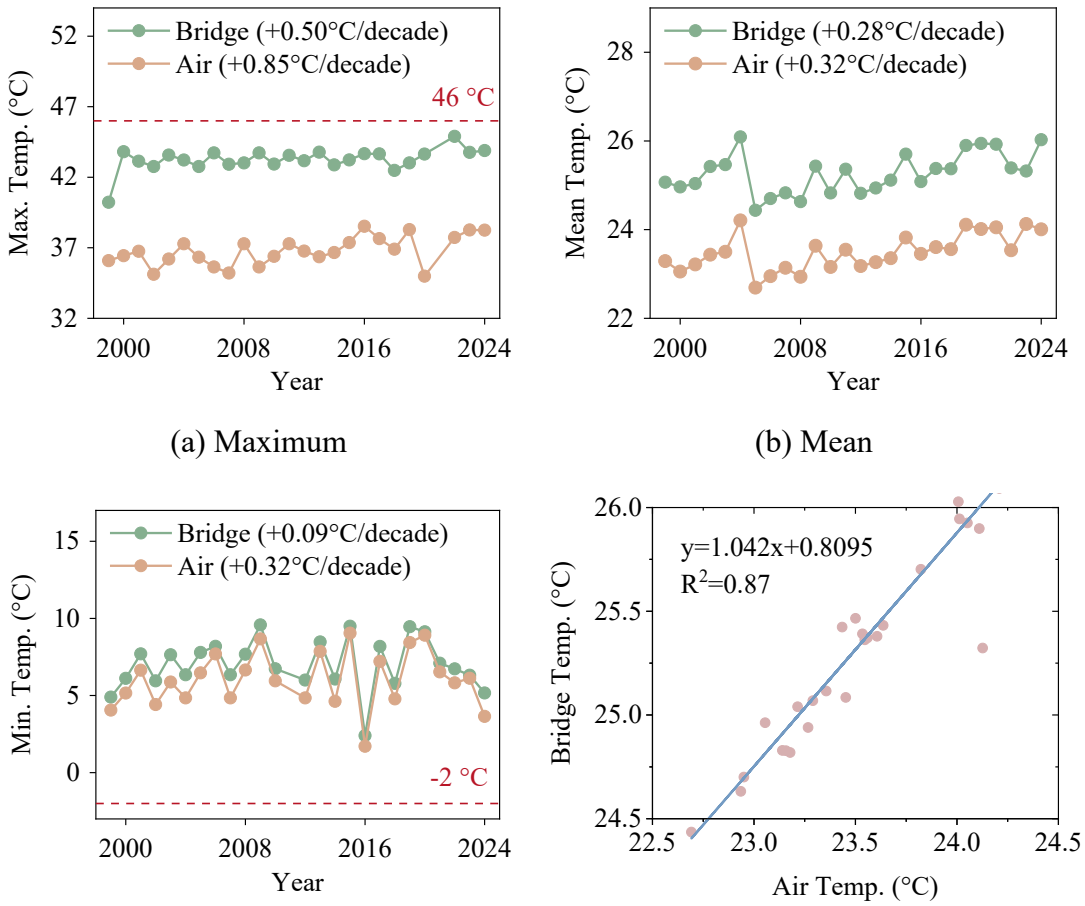

157 Figure 3 Long-term temperature trends of the Tsing Ma Bridge during 1999–2024

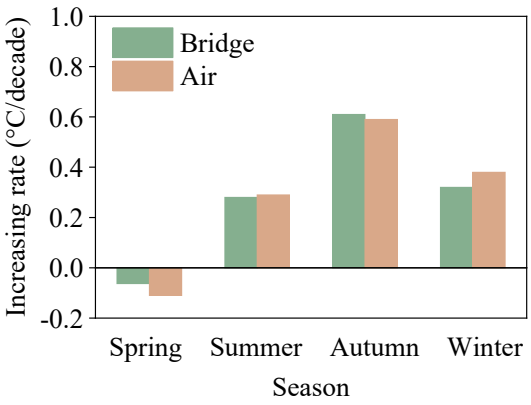

158 Figure 4 Seasonal temperature increasing rates of bridge and air during 1999–2024

4 Changes in extreme heat and frequency

In addition to annual maximum temperatures (1999–2024), the upper-tail distribution of hourly maximum bridge temperatures capturing the shifts in high-temperature patterns is also studied. Figure 5 displays the annual 90th percentile temperatures from 1999 to 2024. The linear regression analysis shows that the temperature increases by 0.53 ℃ per decade. Moreover, the 90th percentile temperature post-2020 (during 2021–2024) is 34.83 ℃, 1.39 ℃ higher than that during 1999–2002 (33.44 ℃). The results indicate accelerated warming in the high-temperature extreme.

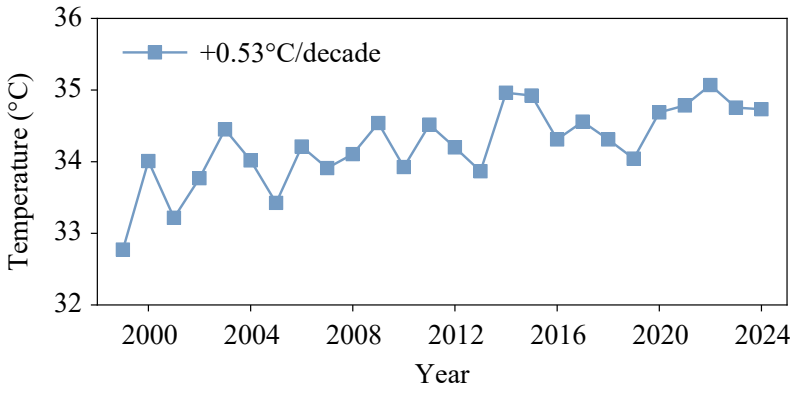

Figure 5 The 90th percentile temperature of hourly maximum temperatures during 1999–2024

Similarly, changes in the frequency of extreme bridge temperature events can reveal underlying warming trends. Therefore, the changing in extreme thermal events should be quantified. The design temperature threshold of the bridge is 46 ℃. Extreme heat events are defined as the daily maximum temperature exceeding 40.25 ℃ (calculated as 75% of the range between the baseline of 23 ℃ and design limit: $23 + (46 - 23) \times 0.75$). Figure 6 gives the number of extreme heat days per year during 1999–2024. The extreme heat events after 2020

(during 2021–2024) is 48 days, while that around 2000 (during 1999–2002) is 17 days only. Therefore, the extreme hot days have increased to 2.8 times the number around 2000. The bridge is at risk of more frequent extreme temperatures.

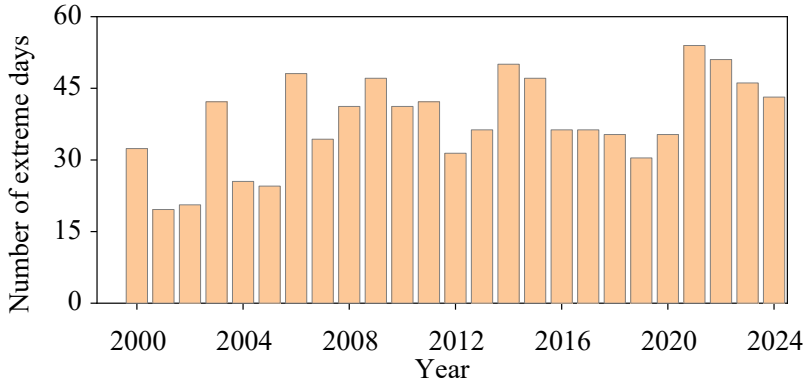

Figure 6 Number of extreme heat days per year during 1999–2024

Air temperature and solar radiation are the key climate factors that affecting bridge temperatures. However, their relative effects have not been studied. In this study, the effects of the daily maximum air temperature and daily total solar radiation on daily maximum bridge temperature are quantified using the standard regression coefficient. The standardized regression coefficient is a dimensionless metric used in the regression analysis to quantify the relative contribution of predictors. It eliminates the effect of differing variable magnitudes through standardization, allowing direct comparison of regression coefficients across variables [54]. The standardized regression coefficient can be calculated as follows:

$$Y = \beta_1 X_1 + \beta_2 X_2 + \varepsilon, \tag{2}$$

$$X'_j = \frac{X_j - \mu_{X_j}}{\sigma_{X_j}} \quad (j = 1, 2), \tag{3}$$

$$Y' = \frac{Y - \mu_Y}{\sigma_Y}, \tag{4}$$

$$\beta'_j = \beta_j \frac{\sigma_{X_j}}{\sigma_Y}, \tag{5}$$

$$Y' = \beta'_1 X'_1 + \beta'_2 X'_2 + \varepsilon', \tag{6}$$

where Y denotes the dependent variable, representing bridge daily maximum temperature in this research; X_1 and X_2 are independent variables, denoting daily maximum air temperature and daily total solar radiation, respectively; μ_{Xj} and μ_Y are the mean value of X_j and Y, respectively; σ_{Xj} and σ_Y indicate their standard deviations; β_j and β'_j correspond to the raw and standardized regression coefficients, respectively; and ε and ε' represent the error term. A larger standardized regression coefficient indicates a greater contribution of the corresponding regressor to variable Y.

Based on Equations (2) to (6), the standardized regression coefficients for air temperature and solar radiation are calculated as 0.81 and 0.19, respectively. Therefore, the air temperature demonstrates its dominant role in governs the bridge thermal dynamics. This finding is consistent with prior evidence of the close parallel between bridge and ambient air temperatures.

Then the quantile regression analysis method is adopted to capture the effects of solar radiation and air temperature across different bridge thermal states [55]. Quantile regression is a statistical analytical method designed to estimate conditional distribution relationships between variables across different quantile levels. Quantile regression enables the examination

of how independent variables influence a dependent variable at specific quantiles (e.g., median, 10th percentile, and 90th percentile) [56–58]. The linear conditional quantile function can be defined as [59]

$$Q_Y(\tau|X) = X\beta_\tau, \tag{7}$$

$$\beta_\tau = \arg\min_{\beta \in \mathbb{R}^K} \sum_{i=1}^{n} (\rho_\tau(Y_i - X_i\beta)), \tag{8}$$

$$\rho_\tau(u) = \begin{cases} \tau|u| & u \geq 0 \\ (1-\tau)|u| & u < 0 \end{cases}, \tag{9}$$

where $Q_Y(\tau|X)$ represents the τth quantile of Y, and β_τ is the quantile regression coefficient vector.

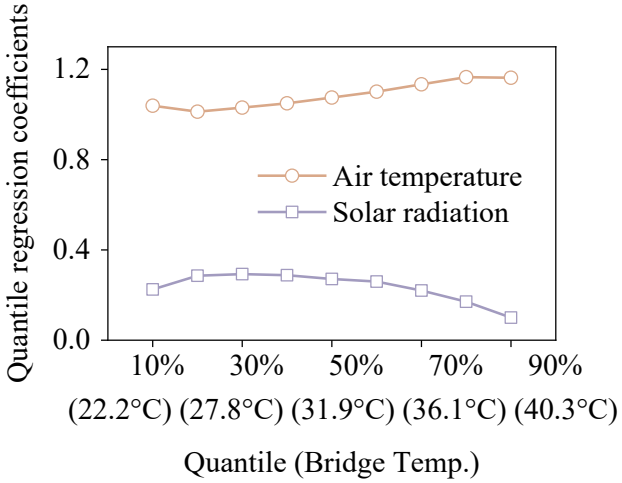

Figure 7 Quantile regression coefficients of air temperature and solar radiation across different bridge temperature quantiles

The quantile regression coefficients of air temperature and solar radiation across different bridge temperature quantiles are calculated and shown in Figure 7. Air temperature coefficients exhibit an increasing trend, rising from 1.04 at the 10% quantile (bridge temperature around 22.2 ℃) to 1.16 at the 90% quantile (bridge temperature around 40.3 ℃), indicating that the influence of air temperature intensifies as the bridge temperatures rise. By contrast, the solar

radiation coefficient reaches its peak of 0.29 at the 20% quantile (bridge temperature around 25.4 ℃) but gradually declines to 0.1 at the 90% quantile (bridge temperature around 40.3 ℃).

5 Verification of bridge extreme high temperature

Extreme high temperatures pose an escalating threat to bridge long term serviceability. According to Figure 3(a), the bridge annual maximum effective temperature has an increasing trend of 0.50 ℃ per decade. To verify this trend is attributable to climate change, the observed warming trend is validated through the heat-transfer analysis and finite element model using climate data from annual hottest days.

5.1 Heat-transfer analysis

Bridges exposed to the external environment undergo heat exchange processes with their surroundings, which directly govern their thermal state. The heat exchange processes include heat conduction, heat convection, and heat radiation. Heat conduction is the transfer of thermal energy from regions of the bridge with higher temperatures to regions with lower temperatures through direct interactions between molecules. Heat convection occurs between the bridge and the surrounding air. Heat radiation comprises direct, diffuse, and reflected solar radiation, along with absorbed atmospheric long-wave radiation and long-wave radiation emitted from the bridge surface, as illustrated in Figure 8.

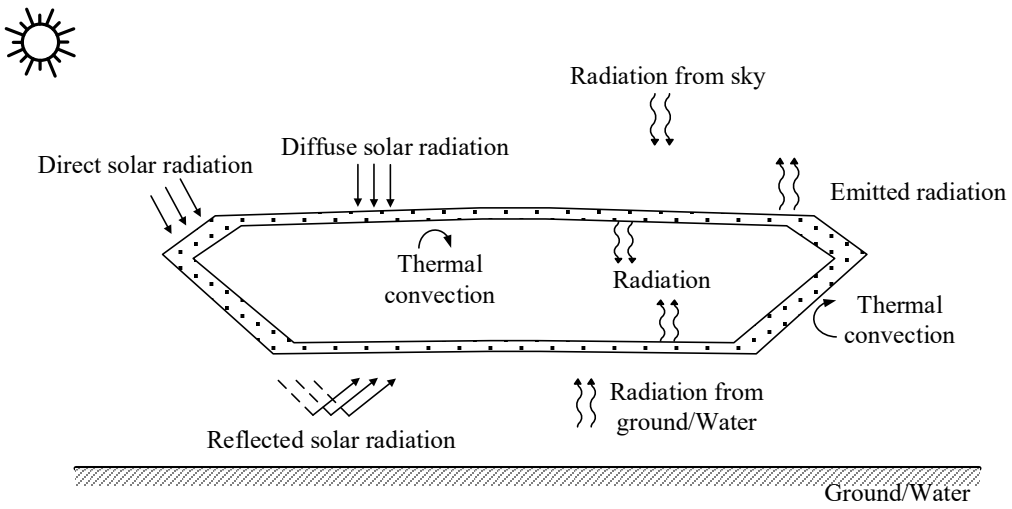

Figure 8 Heat exchange of a bridge exposed to the environment [60]

Given that temperature variations along the longitudinal axis of the bridge are negligible, they are excluded in the analysis. This simplification allows the bridge's thermal boundary conditions to be effectively characterized in two dimensions as [61, 62]:

$$k\left(\frac{\partial T}{\partial x}n_x+\frac{\partial T}{\partial y}n_y\right)+q=0\,, \tag{10}$$

where k represents the coefficient of thermal conductivity, n_x and n_y are the direction cosines of the outer surface, and q represents heat flow defined as [63]

$$q=q_c+q_r+q_s\,. \tag{11}$$

The heat convection q_c, heat irradiation q_r, and solar radiation q_s can be expressed by the following formula:

253 $$q_c = h_c(T_a - T_s), \tag{12}$$

254 $$q_r = G_a + G_g - G_s, \tag{13}$$

255 $$q_s = \alpha I_s, \tag{14}$$

256 $$h_c = \begin{cases} 4 \times w + 5.6 & (w < 5\,\mathrm{m/s}) \\ 7.15 \times w^{0.78} & (w \geq 5\,\mathrm{m/s}) \end{cases}, \tag{15}$$

257 where h_c denotes the convective heat transfer coefficient between the bridge surfaces and air,
258 which is functionally dependent on wind speed w (Equation (7)) [60]; T_a and T_s are the air and
259 structural temperatures, respectively. G_a is the bridge surface's long-wave radiation absorbed
260 from the atmosphere, G_g is that absorbed from the ground, G_s represents the emitted long-wave
261 radiation [60], and I_s is the absorbed solar radiation.

262 **5.2 Finite element model**

263 A finite element model of the Tsing Ma Bridge deck is constructed to validate the observed
264 warming trends. A typical segment of the Tsing Ma Bridge is selected, as shown in Figure 9.
265 The segment is mainly composed of orthotropic deck, cross frame, longitudinal truss, railway
266 beam, and cross bracing, with a total of 40,916 nodes and 33,295 elements. To balance
267 computational accuracy and efficiency, the asphalt pavement layers, orthotropic deck, cross
268 frames, and railway beam are discretized using three-dimensional solid elements, whereas
269 thinner components, such as corrugated webs and cross bracings, are represented by shell
270 elements [64]. Material parameters (e.g., elastic modulus and thermal expansion coefficients)
271 are documented in Table 2 [60].

272 The external surfaces of the bridge account for solar radiation, atmospheric long-wave

radiation, and convective heat transfer, whereas the internal surfaces incorporate long-wave radiation exchanges between interior surfaces and convective heat transfer. These boundary conditions are applied to the bridge model to calculate component temperatures through heat-transfer analysis.

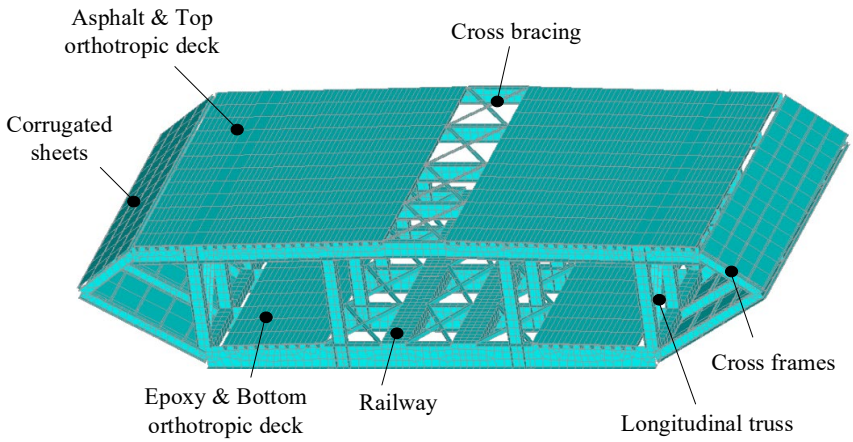

Figure 9 Finite element model of the typical segment of bridge [60]

Table 2 Material properties used in the finite element model [60]

Parameters	Steel	Asphalt
Density	7850	2450
Thermal conductivity	55	2.5
Specific heat capacity	460	960
Elastic modulus	2.05×10^{11}	1.3×10^{9}
Poisson's ratio	0.3	0.2
Emissivity coefficient	0.8	0.92
Absorptivity coefficient	0.685	0.90

The through-length structural components of the bridge cross-section are used to calculate bridge effective temperature, which include the top and bottom bridge orthotropic decks, U trough, and longitudinal trusses, as given in Figure 2.

To mitigate initial condition effects in the heat-transfer analysis, bridge temperatures are simulated for both the annual hottest day and its preceding day. After the heat-transfer analysis in the preceding day, the resulting temperature distribution provides realistic initial conditions for the simulation of the target day. This initialization method effectively eliminates errors caused by assumed initial thermal states.

5.3 Verification results

Using the year of 2023 as an example, July 14, 2023 is the hottest day of the year. The measured air temperature and solar radiation data from July 13 and 14 are applied to the finite element model and perform heat-transfer analysis. The bridge temperatures and solar radiation used for these two days are presented in Figures 10 and 11, respectively.

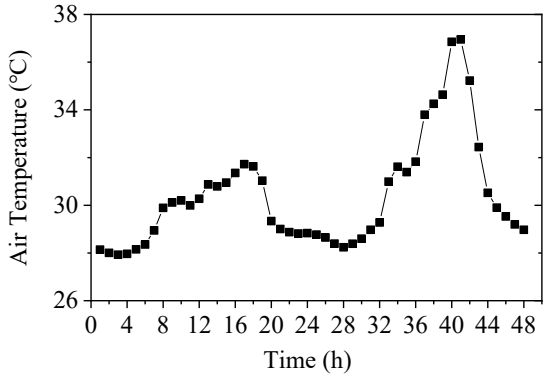

Figure 10 The SHM system measured air temperature on July 13 and 14, 2023

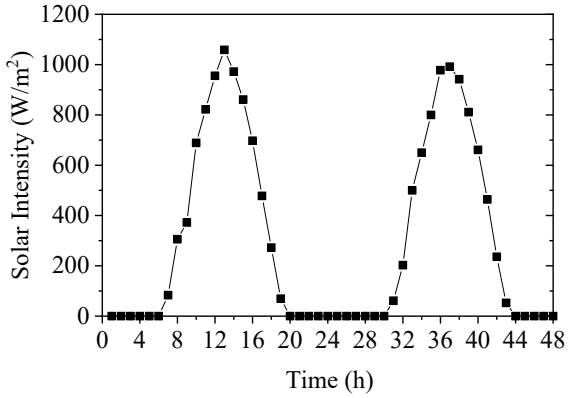

Figure 11 HKO measured solar radiation on July 13 and 14, 2023

Figure 12 compares the calculated and measured temperatures for details A and B (Figure 9), which encompass bridge orthotropic decks and U troughs. The calculated results have a very good agreement with the measurements. The effective temperature of the deck section is then compared with the measurement data in Figure 13. The two sets of data also align well with each other, with a root mean square error (RMSE) of 0.86 ℃. These results demonstrate that the finite element model can accurately simulate thermal behavior of the bridge.

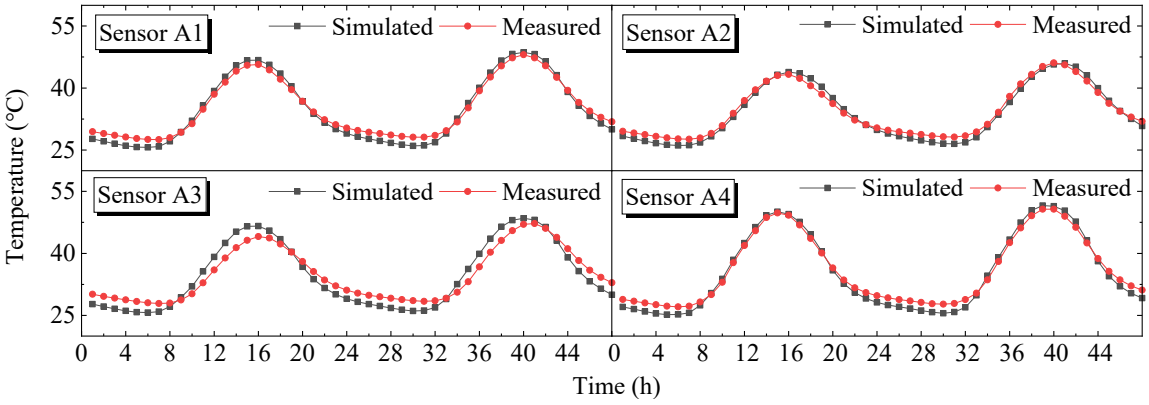

(a) Detail A

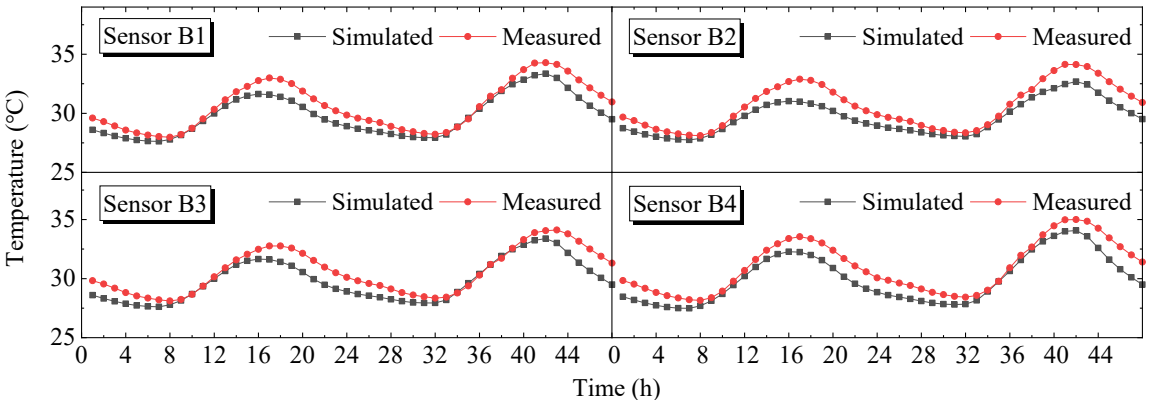

306

307 (b) Detail B

308 Figure 12 Measured and calculated bridge component temperature on July 13 and 14, 2023

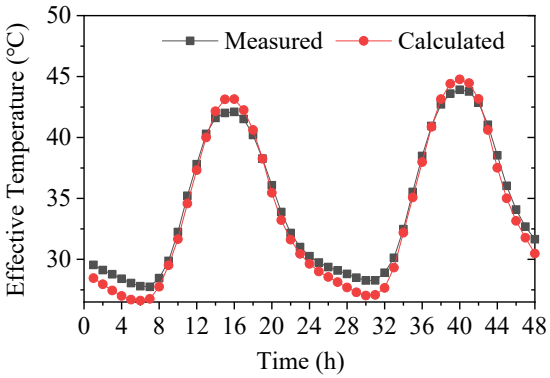

309

310 Figure 13 Measured and calculated bridge effective temperature on July 13 and 14, 2023

311 Finally, the annual maximum effective temperatures of Tsing Ma Bridge in other years of
312 1999–2024 are similarly calculated and shown in Figure 14. The simulated results closely
313 match the observed bridge temperatures during the period, with an average discrepancy of
314 0.92 ℃. Consequently, the numerical simulation results verify the observed temperature
315 increases. Both numerical and monitoring data confirm that climate change causes the
316 temperature increases in the bridge.

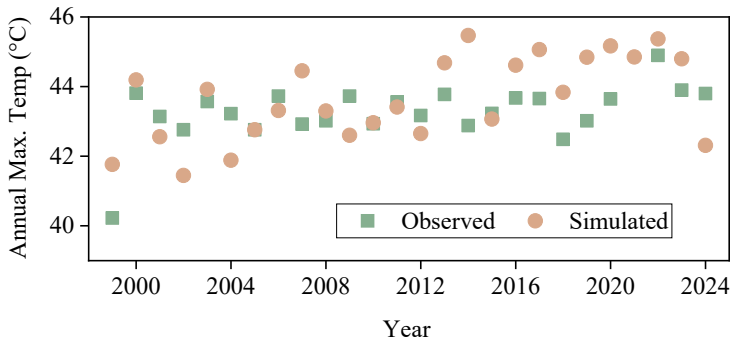

317

318 Figure 14 Measured and calculated annual maximum bridge temperatures during 1999–2024

319 The annual maximum temperature of the bridge in 2022 was 44.9 ℃ (Fig. 2b), nearing
320 the current design threshold (46 ℃). As climate change intensifies over time, bridge
321 temperatures associated with climate change will continue to increase. Extrapolating the
322 observed warming trend during 1999–2024, bridge temperatures are projected to exceed the
323 design limit by 2068. By the end of the bridge's 120-year design service life in 2117 (the bridge
324 was constructed in 1997), temperatures are predicted to rise by an additional 4.65 ℃, reaching
325 48.45 ℃—2.45 ℃ above the design limit. Although such a temperature excess may not
326 immediately result in structural unfavorable conditions, it could accelerate material
327 degradation, pose long-term integrity risks, and increase maintenance costs.

328

329 ## 6 Conclusions

330 Climate change poses potential risks to bridge infrastructure. This study quantifies the
331 impacts of climate change on bridge temperatures by analyzing 26 years of structural health
332 monitoring temperature data for the Tsing Ma Bridge. Some main conclusions can be drawn as
333 below:

1. Climate change has increased both the mean and extreme temperatures of the Tsing Ma Bridge. The annual mean effective bridge temperature rose at 0.28 ℃ per decade, closely following the ambient warming rate (0.32 ℃ per decade). Notably, extreme bridge temperatures escalated 0.50 ℃ per decade, 1.8 times faster than the average increase. The increasement in annual minimum temperature is insignificant.
2. Both extreme heat and frequency have increased at the Tsing Ma Bridge. The 90th percentile temperature after 2020 has risen by 1.39 ℃ relative to the period around 2000. Furthermore, the post-2020 frequency of extreme heat events (daily T_b > 40.25 ℃) surged to 2.8 times the level around 2000, underscoring accelerating upper-tail risks.
3. Standardized regression analysis confirms that ambient air temperature is the dominant driver of bridge temperature dynamics, significantly surpassing the influence of solar radiation. And the quantile regression analysis results indicate that the influence of air temperature intensifies as bridge temperatures rise.
4. With the finite element model and heat-transfer analysis on the annual hottest days, the calculated effective bridge temperatures agree well with the field measurements. This correlation verifies that the observed temperature increases are attributable to climate change.

To mitigate the effects of temperature rise on bridge performance, future research should focus on developing adaptive strategies such as updating the current design code for existing and new bridges, using reflective coatings to reduce solar absorption, and strengthening

355 deficient bridge components.

Acknowledgements

This research was partially supported by the Collaborative Research Fund (Project No. PolyU C5004-23G) and Otto Poon Research Institute for Climate-Resilient Infrastructure (A/C: ZH9D). The authors thank the Highways Department and the Hong Kong Observatory for providing valuable data.

Author Contribution

Lu Zhang: Writing – original draft, Writing – review and editing, Validation, Software

Xiaoyou Wang: Supervision, Writing – review and editing

Zhi-Peng Chen: Writing – original draft, Writing – review and editing

Jing Qiang: Writing – review and editing

Yong Xia: Supervision, Funding acquisition, Writing – review and editing

Declaration of Interest statement

The authors declare no competing interests.

References

[1] Y. L. Xu, Y. Xia. Structural Health Monitoring of Long-Span Suspension Bridges, (2012) CRC Press.

[2] Y. Xia, Y. Zhou. Temperature Behavior of Bridges, (2025) CRC Press.

[3] Y. Wang, Y. Zhan, R. Zhao. Analysis of thermal behavior on concrete box-girder arch bridges under convection and solar radiation, Adv. Struct. Eng. 19 (7) (2016) 1043-1059.

[4] D. Wang, Y. Liu, Y. Liu. 3D temperature gradient effect on a steel-concrete composite deck in a suspension bridge with field monitoring data, Struct Control Hlth. 25 (7) (2018) e2179.

[5] L. Li, B. Chen, L. Zhou, Q. Xia, Y. Zhou, X. Zhou, Y. Xia. Thermal behaviors of bridges—A literature review, Adv. Struct. Eng. 26 (6) (2023) 985-1010.

[6] M. Tong, L. G. Tham, F. T. K. Au. Extreme Thermal Loading on Steel Bridges in Tropical Region, J. Bridge Eng. 7 (6) (2002) 357-366.

[7] M. Zhou, J. Fan, Y. Liu, J. Zhang, X. Duan, S. Lei. Analysis on non-uniform temperature field of steel grids of Beijing Daxing international airport terminal building core area considering solar radiation, Engineering Mechanics. 37 (5) (2020) 46-54,73.

[8] Y. Zhou, Y. Xia, B. Chen, Y. Fujino. Analytical solution to temperature-induced deformation of suspension bridges, Mech. Syst. Signal Proc. 139 (2020) 106568.

[9] S. Huang, C. Cai, Y. Zou, X. He, T. Zhou, X. Zhu. Experimental and numerical investigation on the temperature distribution of composite box girders with corrugated steel webs, Struct Control Hlth. 29 (12) (2022) e3123.

396 [10] Y. Zhou, Y. Xia, Z. Sun, Y. Fujino. Analytical formulation of the temperature-induced
397 deformation of multispan suspension bridges, Struct Control Hlth. 29 (6) (2022) e2937.
398 [11] P. Cornwell, C. R. Farrar, S. W. Doebling, H. Sohn. Structural Testing Series: Part 4,
399 Exp. Tech. 23 (6) (1999) 45-48.
400 [12] H. Sohn, M. Dzwonczyk, E. G. Straser, A. S. Kiremidjian, K. H. Law, T. Meng. An
401 experimental study of temperature effect on modal parameters of the Alamosa Canyon
402 Bridge, Earthq. Eng. Struct. Dyn. 28 (8) (1999) 879-897.
403 [13] H. Li, S. Li, J. Ou, H. Li. Modal identification of bridges under varying environmental
404 conditions: Temperature and wind effects, Struct Control Hlth. 17 (2009) 495-512.
405 [14] Y. L. Xu, B. Chen, C. L. Ng, K. Y. Wong, W. Y. Chan. Monitoring temperature effect
406 on a long suspension bridge, Struct Control Hlth. 17 (6) (2009) 632-653.
407 [15] R. Kromanis, P. Kripakaran, B. Harvey. Long-term structural health monitoring of the
408 Cleddau bridge: evaluation of quasi-static temperature effects on bearing movements, Struct.
409 Infrastruct. Eng. 12 (10) (2016) 1342-1355.
410 [16] Q. Xia, J. Zhang, Y. Tian, Y. Zhang. Experimental Study of Thermal Effects on a Long-
411 Span Suspension Bridge, J. Bridge Eng. 22 (7) (2017) 04017034.
412 [17] J. Mao, H. Wang, D. Feng, T. Tao, W. Zheng. Investigation of dynamic properties of
413 long-span cable-stayed bridges based on one-year monitoring data under normal operating
414 condition, Struct Control Hlth. 25 (5) (2018) e2146.
415 [18] J. Hu, L. Wang, X. Song, Z. Sun, J. Cui, G. Huang. Field monitoring and response
416 characteristics of longitudinal movements of expansion joints in long-span suspension

417 bridges, Measurement. 162 (2020) 107933.
418 [19] Q. Zhu, H. Wang, J. Mao, H. Wan, W. Zheng, Y. Zhang. Investigation of Temperature
419 Effects on Steel-Truss Bridge Based on Long-Term Monitoring Data: Case Study, J. Bridge
420 Eng. 25 (9) (2020) 05020007.
421 [20] Y. Zhou, Y. Xia, Y. Fujino, K. Yamaguchi. Analytical formulas of thermal deformation
422 of suspension bridges, Eng. Struct. 238 (2021) 112228.
423 [21] Y. Xia, B. Chen, X. Zhou, Y. Xu. Field monitoring and numerical analysis of Tsing Ma
424 Suspension Bridge temperature behavior, Struct Control Hlth. 20 (4) (2013) 560-575.
425 [22] Y. Deng, Y. Ding, A. Li. Structural condition assessment of long-span suspension
426 bridges using long-term monitoring data, Earthq. Eng. Eng. Vib. 9 (1) (2010) 123-131.
427 [23] I. Yoon, O. Çopuroğlu, K. Park. Effect of global climatic change on carbonation
428 progress of concrete, Atmos. Environ. 41 (34) (2007) 7274-7285.
429 [24] T. M. L. Wigley. The effect of changing climate on the frequency of absolute extreme
430 events, Clim. Change. 97 (1-2) (2009) 67-76.
431 [25] M. G. Stewart, X. Wang, M. N. Nguyen. Climate change impact and risks of concrete
432 infrastructure deterioration, Eng. Struct. 33 (4) (2011) 1326-1337.
433 [26] S. Talukdar, N. Banthia, J. R. Grace, S. Cohen. Carbonation in concrete infrastructure in
434 the context of global climate change: Part 2—Canadian urban simulations, Cement and
435 Concrete Composites. 34 (8) (2012) 931-935.
436 [27] S. Talukdar, N. Banthia, J. R. Grace. Carbonation in concrete infrastructure in the
437 context of global climate change—Part 1: Experimental results and model development,

438 Cement and Concrete Composites. 34 (8) (2012) 924-930.
439 [28] L. Wright, P. Chinowsky, K. Strzepek, R. Jones, R. Streeter, J. B. Smith, J. Mayotte, A.
440 Powell, L. Jantarasami, W. Perkins. Estimated effects of climate change on flood
441 vulnerability of U.S. bridges, Mitig. Adapt. Strateg. Glob. Chang. 17 (8) (2012) 939-955.
442 [29] E. Bastidas-Arteaga, F. Schoefs, M. G. Stewart, X. Wang. Influence of global warming
443 on durability of corroding RC structures: A probabilistic approach, Eng. Struct. 51 (2013)
444 259-266.
445 [30] O. Khandel, M. Soliman. Integrated Framework for Quantifying the Effect of Climate
446 Change on the Risk of Bridge Failure Due to Floods and Flood-Induced Scour, J. Bridge Eng.
447 24 (9) (2019) 04019090.
448 [31] S. Palu, H. Mahmoud. Impact of climate change on the integrity of the superstructure of
449 deteriorated U.S. bridges, PLoS One. 14 (10) (2019) e0223307.
450 [32] IPCC. Summary for Policymakers. In: Climate Change 2021: The Physical Science
451 Basis. Contribution of Working Group I to the Sixth Assessment Report of the
452 Intergovernmental Panel on Climate Change [Masson-Delmotte, V., P. Zhai, A. Pirani, S.L.
453 Connors, C. Péan, S. Berger, N. Caud, Y. Chen, L. Goldfarb, M.I. Gomis, M. Huang, K.
454 Leitzell, E. Lonnoy, J.B.R. Matthews, T.K. Maycock, T. Waterfield, O. Yelekçi, R. Yu, and
455 B. Zhou (eds.)]. (2021).
456 [33] A. Nasr, I. Björnsson, D. Honfi, O. Larsson Ivanov, J. Johansson, E. Kjellström. A
457 review of the potential impacts of climate change on the safety and performance of bridges,
458 Sustain. Resil. Infrastruct. 6 (3-4) (2021) 192-212.

[34] M. M. Borah, A. Dey, A. Sil. Reliability assessment of a marine bridge structure considering Indian climatic conditions under time-variant loads, Innov. Infrastruct. Solut. 7 (2) (2022) 159.

[35] V. Mishra, A. Sadhu. Towards the effect of climate change in structural loads of urban infrastructure: A review, Sust. Cities Soc. 89 (2023) 104352.

[36] F. T. K. Au, M. Tong, L. G. Tham. Design Thermal Loading for Steel Bridges in Hong Kong, Transactions. 8 (2) (2001) 1-9.

[37] C. Liu, J. T. DeWolf. Effect of Temperature on Modal Variability of a Curved Concrete Bridge under Ambient Loads, J. Struct. Eng. 133 (12) (2007) 1742-1751.

[38] R. Westgate, K. Koo, J. Brownjohn. Effect of Solar Radiation on Suspension Bridge Performance, J. Bridge Eng. 20 (5) (2015) 04014077.

[39] J. Zhu, Q. Meng. Effective and Fine Analysis for Temperature Effect of Bridges in Natural Environments, J. Bridge Eng. 22 (6) (2017) 04017017.

[40] S. Jiang, A. Ye, C. Xiao. The temperature increase in Greenland has accelerated in the past five years, Glob. Planet. Change. 194 (2020) 103297.

[41] P. M. Forster, C. Smith, T. Walsh, W. F. Lamb, R. Lamboll, B. Hall, M. Hauser, A. Ribes, D. Rosen, N. P. Gillett, M. D. Palmer, J. Rogelj, K. von Schuckmann, B. Trewin, M. Allen, R. Andrew, R. A. Betts, A. Borger, T. Boyer, J. A. Broersma, C. Buontempo, S. Burgess, C. Cagnazzo, L. Cheng, P. Friedlingstein, A. Gettelman, J. Gütschow, M. Ishii, S. Jenkins, X. Lan, C. Morice, J. Mühle, C. Kadow, J. Kennedy, R. E. Killick, P. B. Krummel, J. C. Minx, G. Myhre, V. Naik, G. P. Peters, A. Pirani, J. Pongratz, C. Schleussner, S. I.

480 Seneviratne, S. Szopa, P. Thorne, M. V. M. Kovilakam, E. Majamäki, J. Jalkanen, M. van
481 Marle, R. M. Hoesly, R. Rohde, D. Schumacher, G. van der Werf, R. Vose, K. Zickfeld, X.
482 Zhang, V. Masson-Delmotte, P. Zhai. Indicators of Global Climate Change 2023: annual
483 update of key indicators of the state of the climate system and human influence, Earth Syst.
484 Sci. Data. 16 (6) (2024) 2625-2658.
485 [42] Z. Hu, M. J. McPhaden, B. Huang, J. Zhu, Y. Liu. Accelerated warming in the North
486 Pacific since 2013, Nat. Clim. Chang. 14 (9) (2024) 929-931.
487 [43] E. Bevacqua, C. Schleussner, J. Zscheischler. A year above 1.5 °C signals that Earth is
488 most probably within the 20-year period that will reach the Paris Agreement limit, Nat. Clim.
489 Chang. 15 (3) (2025) 262-265.
490 [44] A. J. Cannon. Twelve months at 1.5 °C signals earlier than expected breach of Paris
491 Agreement threshold, Nat. Clim. Chang. 15 (3) (2025) 266-269.
492 [45] M. Wild, H. Gilgen, A. Roesch, A. Ohmura, C. N. Long, E. G. Dutton, B. Forgan, A.
493 Kallis, V. Russak, A. Tsvetkov. From dimming to brightening: decadal changes in solar
494 radiation at Earth's surface, Science. 308 (5723) (2005) 847-50.
495 [46] Y. Qian, D. P. Kaiser, L. R. Leung, M. Xu. More frequent cloud-free sky and less
496 surface solar radiation in China from 1955 to 2000, Geophys. Res. Lett. 33 (1) (2006)
497 L01812.
498 [47] A. Nasr, E. Kjellström, I. Björnsson, D. Honfi, O. L. Ivanov, J. Johansson. Bridges in a
499 changing climate: a study of the potential impacts of climate change on bridges and their
500 possible adaptations, Struct. Infrastruct. Eng. 16 (4) (2020) 738-749.

501 [48] M. Nassar, L. Amleh. The effect of projected air temperatures on concrete box girders
502 thermal gradients and effective temperatures in Canada, Results Eng. 20 (2023) 101453.
503 [49] S. Saad, A. Nasir, R. Bashir, S. J. Pantazopoulou. Numerical Study on the Effect of
504 Climate Parameters on the Extreme Thermal Gradients in Concrete Box Girders, J. Bridge
505 Eng. 28 (10) (2023) 04023069.
506 [50] K. Y. Wong, C. K. Lau, F. A. R. Planning and implementation of the structural health
507 monitoring system for cable-supported bridges in Hong Kong, Nondestructive evaluation of
508 highways, utilities, and pipelines IV. (2000) 266-275.
509 [51] Y. Xu. Making good use of structural health monitoring systems of long-span cable-
510 supported bridges, J. Civ. Struct. Health Monit. 8 (3) (2018) 477-497.
511 [52] L. Zhang, T. Lu, F. Wang, Y. Xia. Over 25-year monitoring of the Tsing Ma suspension
512 bridge in Hong Kong, J. Civ. Struct. Health Monit. (2024).
513 [53] Y. L. Xu, B. Chen, C. L. Ng, K. Y. Wong, W. Y. Chan. Monitoring temperature effect
514 on a long suspension bridge, Struct Control Hlth. (2009) 632-653.
515 [54] A. F. Siegel (2012), "Multiple Regression: Predicting One Variable from Several
516 Others", *Practical Business Statistics.* Elsevier, pp. 371-431.
517 [55] A. Grinsted. quantreg(x,y,tau,order,Nboot), MATLAB Central File Exchange. (2025).
518 [56] R. Koenker, G. B. Jr. Regression quantiles, Econometrica: journal of the Econometric
519 Society. 46 (1) (1978) 33-50.
520 [57] B. S. Cade, B. R. Noon. A Gentle Introduction to Quantile Regression for Ecologists,
521 Front. Ecol. Environ. 1 (8) (2003) 412-420.

[58] Y. Wei, A. Pere, R. Koenker, X. He. Quantile regression methods for reference growth charts, Stat. Med. 25 (8) (2006) 1369-1382.

[59] S. Buhai. Quantile Regression: Overview and Selected Applications, Ad Astra. (2005) 1-17.

[60] L. Zhang, Y. Shan, L. Li, F. Wang, Y. Xia. Thermal boundary conditions for heat transfer analysis of bridges considering non-uniform distribution of internal air temperature by computational fluid dynamics, J. Civ. Struct. Health Monit. 14 (5) (2024) 1295-1310.

[61] S. Whitaker. Fundamental Principles of Heat Transfer, New York (1977) Pergamon Press.

[62] M. M. Elbadry, A. Ghali. Temperature variations in concrete bridges, J. Bridge Eng. 109 (1983) 2355-2374.

[63] T. L. Bergman, T. L. Bergman, F. P. Incropera, D. P. DeWitt, A. S. Lavine. Fundamentals of Heat and Mass Transfer, sixth edition, (2006) John Wiley & Sons.

[64] ANSYS 19.0. [Computer Software]. Southpointe, PA, USA.